A Sequence-Rule Analysis of Active and Passive *LCL* Filters for Three-Phase Inverter-Grid Connection for Damping Stability Consideration

Ronald Jackson*‡, Shamsul Aizam Zulkifli*‡, Suriana Salimin*

*Department of Electrical Power Engineering, Faculty of Electrical and Electronic Engineering, Universiti Tun Hussein Onn Malaysia, 86400 Parit Raja Batu Pahat, Johor, Malaysia

(ronaldjackson91@yahoo.com, aizam@uthm.edu.my, suriana@uthm.edu.my)

‡ Ronald Jackson and Shamsul Aizam Zulkifli, Department of Electrical Power Engineering, Faculty of Electrical and Electronic Engineering, Universiti Tun Hussein Onn Malaysia (UTHM), 86400 Parit Raja, Batu Pahat, Johor, Malaysia, Tel: +6074537559, Fax: +6074538387, ronaldjackson91@yahoo.com, aizam@uthm.edu.my

Received: 08.04.2020 Accepted: 10.05.2020

Abstract- This paper delivers the step sequence that complies with the systematic design methodology for the *LCL*-type filter for the inverter-grid system, as well as an analysis of its internal damping stability. The use of the power inverter is vital to transfer the energy from renewable energy sources to the existing electrical grid. Therefore, it is essential to model a non-response *LCL* filter's parameter values that do not compromise the filter's effectiveness and provide pure current waveform for harmonics reduction before the current is injected into the grid. At the same time, the *LCL* filter also must have a stable damping performance that is able to attenuate the high resonance peak and simultaneously offers better high-frequency attenuation. To verify the selected inductance and capacitance values of the *LCL* filter, passive and active damping methods are comparatively studied. Each step provided in this paper for the modeling and selection of vulnerable coefficients of the *LCL* filter is verified through MATLAB/Simulink software, and simulation results show significant evidence that the sequence will give a better signal current output, maintain the cutoff frequency signal and reduce the Total Harmonics Distortions (THD) to below the IEEE Standard.

Keywords *LCL* filter, passive, active, internal damping, stability.

1. Introduction

In the current paradigm of a power system, distributed power generation (DG) systems have been widely realized for the integration of renewable energy sources (RES). It is because renewable energy has become a promising source of alternative energy generation which significantly solves the current energy crisis and environmental concerns by delivering more sustainable energy as well as reducing global warming, as reported in decarbonization policies [1]. A grid-connected inverter controlled by pulse-width modulation (PWM) techniques has an extensive impact in promoting RES consumption, where the power converter is used as an interface unit that enables RES to deliver power to the power grid. Hence, it is vital to identify which filter types are adequate for each application. The accessibility of RES operation is necessary due to the power electronic-interfaced converter acting as the voltage source inverter (VSI) that can operate in two different modes, which are the voltage-controlled mode (VCM) and the current-controlled mode (CCM) [2]–[4]. In VCM, the VSI output is controlled by regulating its amplitude and frequency. On the other hand, CCM adjusts the output current to the reference value. İndeed, with this accessibility, more advanced distributed electrical systems with multiple-source DGs and loads, which are defined as microgrids, can be regulated at the same time. This will not be discussed in this paper.

An interfaced inverter decoupled with an AC low-pass passive filter is primarily used to attenuate high current harmonics injected into the primary grid. Three types of low-pass filters have been presented over the years, which are *L*, *LC* and *LCL* filters. Undoubtedly, the *L* filter is the most commonly applied filter due to its direct implementation, followed by the *LC* and *LCL* filter configurations. However, the *L* filter experiences a higher inductance value and gives low attenuation [5], making it vulnerable to harmonics pollution at high switching frequency. Therefore, the *LC* filter is presented to overcome the limitations of the *L* filter. Better attenuation and less losses, as well as cost reduction, are the main advantages of the *LC* filter. Despite these advantages, the resonance frequency of the *LC* filter is proportional to the grid's inductance value [6], thus making it not compatible with grid-connected inverter applications. Hence, the *LCL* filter is used to decouple the inverter from the primary grid. It provides a great extent of attenuation at higher inverter switching frequency, while at the same time having low grid inductor current ripples [7], [8]. For instance, if the PWM's switching/carrier frequency, f_{sw}, is at 10 kHz, then the cutoff frequency, f_c, is relatively smaller than 10 kHz to provide enough attenuation for the harmonics near to 10 kHz. Both the *L* and *LC* filters are not recommended because the reduction of high-frequency attenuation is rated at −20dB/dec and at −40 dB/dec, respectively [5], [9]. Whereas, the *LCL* filter's harmonics attenuation can achieve −60dB/dec with small values of inductance and capacitance.

Numerous studies have been presented for the designing of the *LCL* filter with better stability. For instance, the research in [5], [6], [10]–[15] propose modeling and stability approaches through the interactivity within the microgrid with filter implementation, which is claimed as invulnerable to higher-harmonics attenuation and with small values of inductance and capacitance required. It offers flexibility to the control design and the tuning process, particularly for the inner control loop. Meanwhile, studies in [16] and [17] shows the harmonics pollution can be attenuated through renewable energy generator itself. Yet this approached experience high computational burden. The *LCL* filter is predominantly used for the reduction of harmonics pollution by a great extent, yet it broadens the stability issues. Hence, the passive and active damping methods are included to damp the resonance [18], [19]. This means that an adequate filter design methodology can be maximized with avoidance of undesirable stability issues. Although systematically designed, the *LCL* filter-based grid-connected inverter experiences additional stability issues. The overall system stability may be degraded with the presence of the external resonance through the inverter and the weak grid and also from the configurations of the inverters in parallel, so-called the external stability phenomenon. Whereas, the stability of the internal current control loop is equivalent to the inherent *LCL*-filter's resonance peak, which corresponds to the internal stability. Numerous research works have been presented to provide solutions to overcome the *LCL* filter's resonance. For instance, the standard solution for this phenomenon is by adopting the passive damping (PD) method. In such a way, the resonance peak can be attenuated by adding a resistor in series with the capacitor and in parallel with the inductor of the *LCL* filter, while at the same time providing enormous current controller stability by widening the frequency range [11]. It offers a more straightforward implementation with sufficient resonance attenuation. However, it requires a resistor (physical), which provides high damping losses, increases power losses to the system and increases the filter's size, while the reliability of the passive components becomes degraded.

Numerous works have been proposed to provide a more efficient solution than the conventional PD method. For instance, the active damping method (AD) has become an alternative method to mitigate the *LCL* filter's resonance phenomenon. In contrast with the PD method, the AD approach is realized without adding extra sensors as well as passive parameters. However, there are still research gaps in the sequence-rule analysis of passive and active grid-connected *LCL* filters. Therefore, along with presenting filter-designing procedures, this paper provides a comparative study of the step sequence for active and passive damping methods since they rigidly bond to inverter control for actively damped oscillations between the output filters. Hence, this paper contributes towards legitimate guidelines for parameters boundary selection for stability and do not interfere with the output signal for designer to plan their filter that meet the requirement. A typical *LCL* filter-based inverter-grid system, which includes the inverter-side inductor L_f, the grid-side inductor L_g and the capacitor C_f, is shown in Fig. 1.

The remainder of this paper is organized as follows. Section 2 delivers a systematic design methodology for the *LCL* filter with relevant procedures for the design process. Section 3 presents the discussion on the damping stability techniques, including passive and active damping methods, while providing characteristics comparison in a tabulated study. Simulation results for both damping methods are presented in Section 4, and the conclusion is delivered in Section 5.

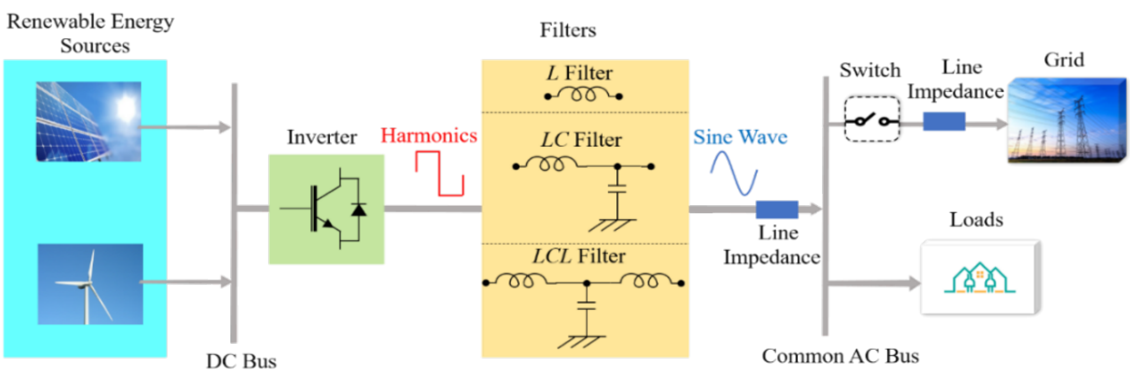

Fig. 1 Microgrid with grid-connected inverter

2. *LCL*-Filter's Systematic Design Methodology

Various criteria should be considered when designing an *LCL* filter, for instance, the filter size, the switching ripple attenuation and the current ripple. Therefore, the per-phase equivalent circuit is presented in Fig. 2, which can extract the derivative equations via Kirchhoff's voltage and current laws, as stated below:

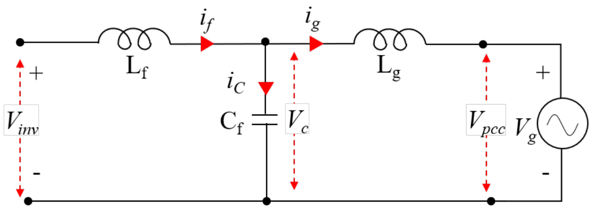

Fig. 2 The per-phase equivalent circuit of the *LCL* filter

$$\left.\begin{aligned} V_{L_f}(s) &= V_{inv}(s) - V_c(s) \\ i_c(s) &= i_f(s) - i_g(s) \\ i_g(s) &= \frac{V_c(s) - V_g(s)}{sL_g} \end{aligned}\right\} \quad (1)$$

At the initial stage, all the initial conditions should be predetermined, including the line-to-line voltage V_{rms}, base power P_b, inverter switching frequency f_{sw}, grid/rated frequency f_g and rated current I_{rated}. Then, the parameter selection of the *LCL* filter can be realized as stated below.

<u>*Step 1*</u>*:* Determine the filter capacitance's base value, C_b. The filter capacitance C_f can be obtained as 5% of the base capacitance, or $C_f = 0.05C_b$.

<u>*Step 2*</u>*:* Determine the inverter-side inductance L_f with the maximum current ripple at the inverter ΔI_{Lmax} with modulation index m:

$$\Delta I_{L\max} = \frac{2V_{dc}}{3L_f}(1-m)mT_{sw} \quad (2)$$

The maximum peak-to-peak current ripple is believed to occur at m=0.5; thus, the equation can be derived as:

$$\Delta I_{L\max} = \frac{V_{dc}}{6f_{sw}L_f} \quad (3)$$

By selecting 10% ripple of the rated current, I_{max} is given by:

$$\Delta I_{L_{\max}} = 10\% \frac{P_b\sqrt{2}}{3V_{ph}} \quad (4)$$

<u>*Step 3*</u>*:* Select harmonics attenuation factor δ at 20% within $(10\% \le \delta \le 30\%)$ [20]; thus, L_g can be determined accordingly:

$$L_g = \frac{\sqrt{\frac{1}{\delta^2}+1}}{C_f\left(2\pi f_{sw}\right)^2} \quad (5)$$

or L_g can be obtained through the ratio (κ) of L_g and L_f, where L_g=κL_f, and L_g can be defined either less than L_f, or similar to L_f when achieving κ=1.

<u>*Step 4*</u>*:* Verify that the resonance frequency f_r must be within an acceptable range. If f_r is less than $10f_g$, then the capacitance value in Step 1 should be reduced. Whereas, when f_r is higher than the $0.5f_{sw}$, either the capacitance value or f_{sw} should be amplified.

$$f_r = \frac{1}{2\pi}\left(\sqrt{\frac{L_f + L_g}{L_f L_g C_f}}\right) \quad (6)$$

<u>*Step 5*</u>*:* Check that the Total Harmonics Distortion (THD) of f_g should be lower than 5%. If higher, then adequately reduce δ with a new design process.

The selection of the *LCL* filter's parameters is an iteration process until all the constraints are satisfied. Table 1 displays the respective burden of the *LCL* filter's parameter values on filter performance. The validation of these values is carried out via the internal stability process in Section 3 and the simulation is presented in Section 4.

Table 1 The performance burden of *LCL* filter's parameters

Parameters	Performance burden
Filter capacitance, C_f $C_f = 5\%\left(\frac{P_b}{2\pi f_g V_{rms}^2}\right)$	Small C_f involves large inductance. Large C_f is consequential in low power factor.
Inverter-side inductance, L_f $L_f = \frac{V_{dc}}{6f_{sw}\Delta I_{L_{\max}}}$	Large L_f results in high voltage drop that is less than the current ripple.
Harmonics attenuation rate, δ $\delta = \frac{1}{1+\kappa\left(1-L_f C_f \omega_{sw}^2\right)}$	Small δ is equivalent to having low THD.
Resonant frequency, f_{res} $10f_g < f_{res} < 0.5f_{sw}$	Small f_{res} corresponds to narrow control bandwidth. Large f_{res} involves resonance peak near f_{sw}.
Damping resistance, R_d $R_d = \frac{1}{3\omega_r C_f}$	Large R_d results in high losses.

2.1. Example of a generalized design procedure

Based on the discussion above, the parameter values and the generalized design procedure for the *LCL* are now presented comprehensively for scalability. Thereby, the values for both inductance and capacitance would be selected accordingly. The chosen inverter with base power P_b of 5 kW is used, together with 400 V_{dc} of DC-link voltage, 12 kHz of inverter switching frequency and a nominal grid system of 240-V 50-Hz three-phase network. The base capacitance C_b can be found as 1.1 mF and the selected capacitance size is 221 µF in order to be within the limit of 5% of the base value C_b. With 10% allowed ripple, equation (4) gives the inverter-side inductance L_f equal to 2.8 mH. After setting the desired attenuation rate δ at 20% and applying equation (5), the grid-side inductance L_g is selected at 4.7 µH. Table 2 summarizes the selected *LCL* parameters with their respective values.

Table 2. The *LCL* filter's selected values

Parameters	Symbol	Value
Base		
Power	P_b	5 kW
Nominal voltage	V_{rms}	240 V
Nominal frequency	f_g	50 Hz
Switching frequency	f_{sw}	12 kHz
Calculated		
Inverter-side inductance	L_f	2.8 mH
Grid-side inductance	L_g	4.7 µH
Capacitance	C_f	221 µF
Resonance frequency	f_r	4.9 kHz

3. Damping Techniques for Internal Stability

As aforementioned, the *LCL*-filter's resonance peak is primarily the factor that distributes the stability of the internal current control loop for the individual inverter. Therefore, numerous damping methods have been discussed over the years that can be employed to escalate the system damping for solving the resonance problem, including the passive damping (PD) and active damping (AD) methods. Henceforth, in this section, further description of the characteristics of both damping methods will be discussed.

3.1. Passive Damping (PD)

The PD method is a widely adopted method to guarantee the stability of *LCL*-filter-based inverter-grid converter. It has been reported that six typical PD methods can be employed by adding serial or parallel resistors in the *LCL* filter branches, as illustrated in Fig. 3. As can be seen, R_{D1}, R_{D3} and R_{D5} are damping resistors in series with L_f, C_f and L_g, respectively. Meanwhile, R_{D2}, R_{D4} and R_{D6} are damping resistors in parallel with L_f, C_f and L_g, respectively. Also, notice that R_1 and R_5 correspond to the equivalent resistances of L_f and L_g. A serial resistor with the capacitor is used to attenuate a portion of the ripple on the switching frequency for resonance avoidance. The selection of the damping resistor's value falls within one-third of the filter capacitor impedance at the resonant frequency [21] to satisfy the requirement in Table 1.

It is worth mentioning that PD_1, PD_3 and PD_5 are relatively common in the PD method as they are equivalent to the resistance for both L_f and L_g inductances as well as the capacitance of C_f. Yet, PD_3 is the sole primary approach applied in grid-connected filters. As compared with PD_3, both PD_1 and PD_5 cause significant damping loss factor due to the path of the power flux directly through R_{D1} and R_{D5} [22]. In addition, the presence of the diminished low-frequency gain causes the dynamic tracking performance to deteriorate. Therefore, PD_1 and PD_5 are not recommended. Meanwhile, from the perspective of damping effectiveness, filtering performance and power losses, PD_3 utilizes a small resistance value, which is not applicable in the other PD methods. At the same time, however, it degrades the attenuation of high-frequency harmonics [23].

In the inverter-grid connection, the voltage source from the power grid is assumed to be an ideal voltage source that contains a pure sinusoidal signal capable of dumping all the harmonics frequencies. Hence, the typical transfer function for the undamped *LCL* filter as grid current per inverter-side voltage is denoted as:

$$G_i = \frac{i_g}{V_{inv}} = \frac{1}{L_f L_g C_f s^3 + \left(L_f + L_g\right)s} \tag{7}$$

The passively damped method becomes a second-order low-pass filter (LPF) at the high-frequency range, thus reducing the harmonics-attenuation ability. Notice that each resistor corresponds to its respective PD method; for instance, R_{D1} is equivalent to PD_1. Thus, each PD method has its respective transfer function which is equivalent to the configuration in Fig. 3. For example, equation (2) represents the transfer function of PD_1, which considers the resistor damping factor. Theoretically, adding a damping resistor could counteract the high resonance peak.

$$G_{PD_1} = \frac{1}{L_f L_g C_f s^3 + L_g C_f R_1 s^2 + \left(L_f + L_g\right)s + R_1} \tag{8}$$

$$G_{PD_2} = \frac{L_f s + R_2}{L_f L_g C_f R_2 s^3 + L_f L_g s^2 + \left(L_f + L_g\right)R_2 s} \tag{9}$$

$$G_{PD_3} = \frac{C_f R_3 s + 1}{L_f L_g C_f s^3 + \left(L_f + L_g\right)C_f R_3 s^2 + \left(L_f + L_g\right)s} \tag{10}$$

$$G_{PD_4} = \frac{R_4}{L_f L_g C_f R_4 s^3 + L_f L_g R_4 s^2 + \left(L_f + L_g\right)R_4 s} \tag{11}$$

$$G_{PD_5} = \frac{1}{L_f L_g C_f R_5 s^3 + L_f C_f R_5 s^2 + \left(L_f + L_g\right)s + R_5} \tag{12}$$

$$G_{PD_6} = \frac{R_6 + L_2 s}{L_f L_g C_f R_6 s^3 + L_f L_g s^2 + \left(L_f + L_g\right)R_6 s} \tag{13}$$

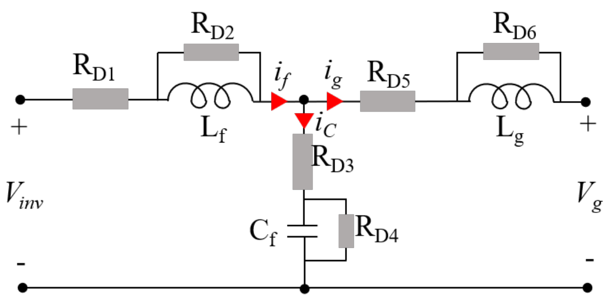

Fig. 3 The configuration of six damping resistors for a typical PD method

3.2. Active Damping (AD)

The active damping approach is generally a filter-based damping method. By inserting a digital LPF filter equivalent to the current control loop, it is used to counteract the resonance peak with a straightforward implementation without additional sensors and passive components. In addition, it can be directly cascaded into the current controller. Numerous filters have been proposed, including notch filter (NF) [18], [24] and low-pass filter [12], [25], among others.

For the NF approach, the compensation of resonance peak is realized by inserting an NF in the current loop to introduce a negative notch peak in the system. In order to provide adequate damping, the tuning of NF frequency, f_n, has to be at the resonance frequency of the *LCL* filter, or f_n equal to f_r [24]. Therefore, f_n is tuned to differ from the nominal f_r to emulate the parameters' shift. The merits of the NF method is that it offers a sensorless concept, along with requiring no passive component. However, the design solely depends on the inductance and capacitance values of the *LCL* filter. Despite offering system stability and robustness, it still has inherent limitations. For instance, the phase deviation causes stability deterioration, and estimation accuracy is still affected by the system model. In addition, the notch effect depends on the resistance of the *LCL* filter; thus, it is vital to know the resistance values of the inductors [26]. Hence, LPF is chosen over the notch filter as it offers superior stability performance as well as design simplicity. The system transfer function for high frequency is unaffected and even contains the notch filter function. The transfer function of NF is denoted as follows:

$$G_N(s) = \frac{s^2 + \omega_n^2}{s^2 + Qs + \omega_n^2} \quad (14)$$

where Q and ω_n correspond to notch filter quality factor and angular frequency of notch, respectively. Notice that Q is equivalent to a narrow rejection bandwidth that results in sensitivity to the shifting of resonance frequency by a great extent [19].

As compared with the NF method, the LPF method significantly widens the phase margin of the system that corresponds to f_r [27]. The selection of the filter's cutoff frequency f_c is a tradeoff between the control bandwidth and the stability margin. Consequently, the low resonance frequencies can be damped out but owing to the diminished closed-loop bandwidth. However, the better tradeoff is observed when the selection of cutoff frequencies is equal to resonance frequencies, or $w_c=w_r$ [25]. Therefore, the sufficient damping coefficient is selected at 0.77, or 1/√2. The advantage of the active damping method is that it can bypass the −180° crossing in the frequency range with a gain above 0 dB. Thus, the −180° crossing can be reduced and shifted either to lower or higher frequencies. The standard LPF second-order transfer function is denoted as below:

$$G_s = \frac{\omega_r^2}{s^2 + 2\xi\omega_r s + \omega_r^2} \quad (15)$$

where ω_r corresponds to the angular resonance frequency of the *LCL* filter and ζ is the damping coefficient. By using the parameter values shown in Table 2, with damping resistance of $0.1\ \Omega \le R_D \le 10\ k\Omega$, damping factor of $0.3 \le \zeta \le 0.7$ and resonance frequency f_r at 4900 Hz, the corresponding adequate damping stability is when considering the 0.7 damping factor.

4. Simulation Results

The passive and active damping methods' performances are tested thoroughly using MATLAB/Simulink. For this purpose, the *LCL* filter's parameters listed in Table 2 are used. The system is supplied with 240-V_{rms} 50-Hz three-phase sinusoidal supply. Both damping methods are comparatively presented to address the attenuation of resonance peak and the reduction of high-frequency harmonics.

4.1. Passive damping analysis

The Bode plots of the *LCL* filter's frequency response for undamped and damped stability via the PD method, which are based on the transfer functions in equations (2) to (7), are depicted in Fig. 4. As can be seen, the undamped results have a higher resonance peak that leads to instability issues. Conversely, it can be counteracted by applying various damping resistance values. As noticed in Fig. 4(b), (c) and (f), the attenuation slope of the high frequency is diminished in comparison with the undamped *LCL* filter. This is due to the zero component in the transfer function.

Meanwhile, Fig. 4(a) and (e) show that the attenuation of high-frequency harmonics is unaffected but causes significant damping losses in PD_1 and PD_5, which are introduced by the direct path of the power flux via R_1 and R_5. Thus, the dynamic performance is reduced, caused by a reduction in the low-frequency gain. Therefore, PD_1 and PD_5 are not suitable and not recommended. Meanwhile, PD_2 and PD_6 require large resistance values with condensed harmonics-attenuation ability. In comparison, the filtering performance shown by PD_4 is adequate as compared with the other five PD methods and with constant frequency characteristics, yet its damping losses are comprehensively high due to the effect of AC bus voltages.

Comparing the six typical PD methods, PD_3 illustrates the most effective damping, better filtering performance and less power losses. Notably, it solely uses small resistance values, but this deteriorates its attenuation of high frequency. Therefore, R_3 is selected as 20% of the capacitor impedance at the resonance frequency to provide ample stability margin for the system. However, power losses are inevitable in PD_3. Nevertheless, the currents passing through damping resistor R_3 can be embedded into the switching harmonics, resonance components and fundamental variables; thus, power losses are primarily caused by the resonance and fundamental currents. PD_3 is relatively recommended since it can gradually reduce damping losses while retaining the attenuation of high-frequency harmonics.

Although the PD method can ensure a robust system along with stability, it still has inherent limitations that affect the effectiveness of the overall system in terms of damping losses. The merits and shortcomings of the six typical PD methods according to Bode plots obtained in Fig. 4 are comprehensively presented in Table 3.

4.2. *Active damping analysis*

Digital filter-based active damping is applied for passive component avoidance and better high-frequency stability performance. After employing the filtered active damping method, the *LCL* filter's resonance peak is counteracted, as proved through the Bode diagrams shown in Fig. 5. Also, notice that the *L* filter's transfer function feature is being included. The *L* filter is well known to have a simple design by excluding the capacitive shunt branch and retaining the inductance values. The *LCL* filter is well-damped when applying the damping coefficient ζ in the transfer function in equation (15) under various damping factors and implementing the parameters listed in Table 2. In Fig. 5(a), notice that the damping coefficient ζ increases from 0.3 to 2. Notice also that up to a sufficient value, which is selected at 0.7, it has the ability to attenuate the high-resonance frequency. Meanwhile, Fig. 5(b) shows the stability margin in the root locus diagram. Notice that the conjugates move to the left-plane as the damping coefficient increases. It proves that the designed *LCL*'s parameter values show stable characteristics, along with an increased damping coefficient. As a result, superior stability is obtained at this stage. Hence, better stability for L_f, L_g and C_f is guaranteed even under various damping coefficients.

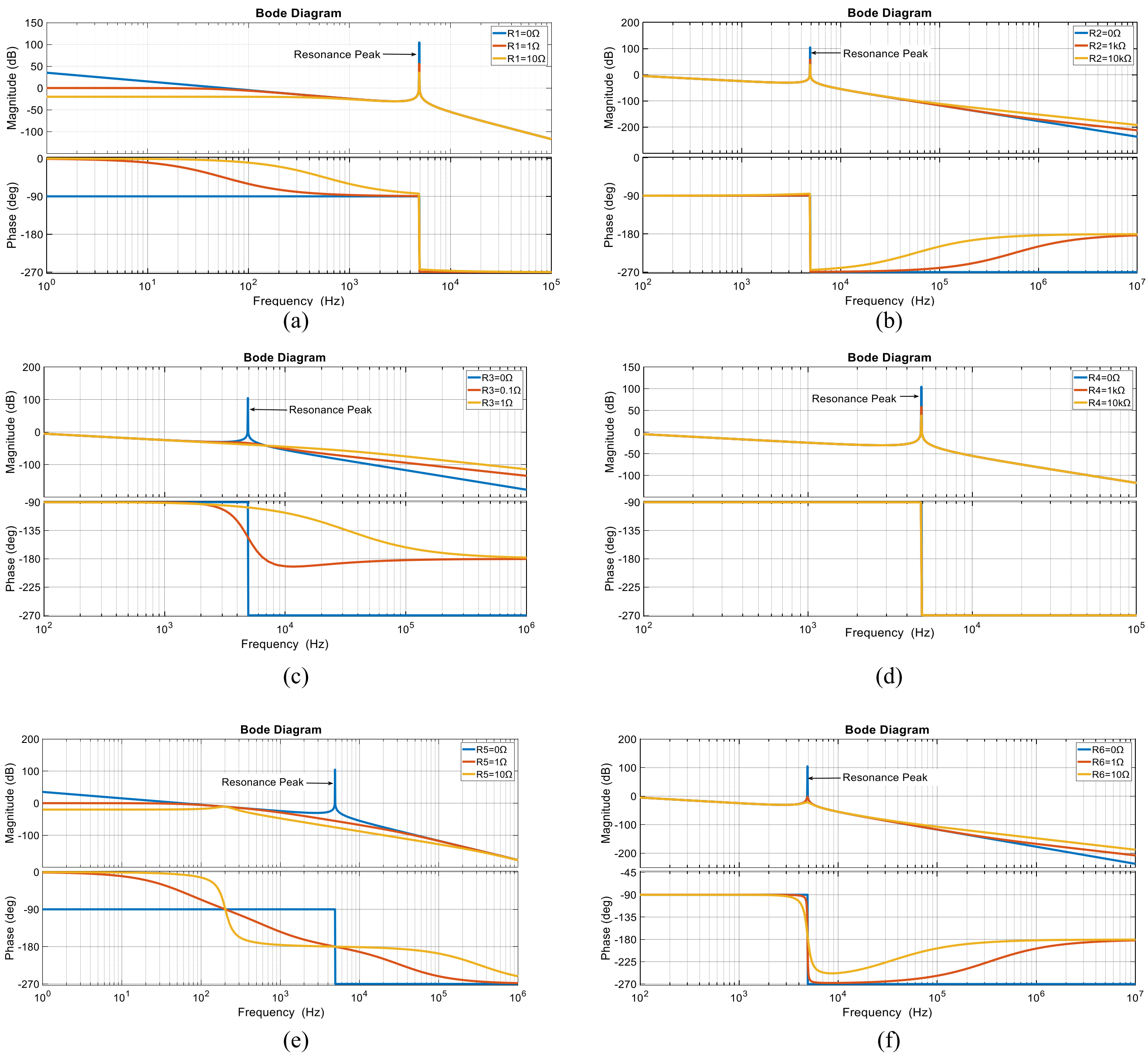

Fig. 4 Bode plots for passive damping methods with various damping resistor values: (a) PD_1, (b) PD_2, (c) PD_3, (d) PD_4, (e) PD_5 and (f) PD_6

Table 3 The benefits and shortcomings of the damping method

Damping methods	Benefits	Shortcomings
PD_2	Better low-frequency gain.	Damping loss factor. Experiences damping losses.
PD_3	Better low-frequency gain. Small number damping resistor is required.	Damping loss factor. Deterioration of high-frequency harmonics attenuation performance.
PD_4	Better damping performance. Better low-frequency gain.	Higher degree of damping losses. Modest capability of disturbance rejection.
PD_6	Better low-frequency gain. Fast dynamic response.	Higher degree of damping losses. Deterioration of high-frequency harmonics attenuation performance.
AD	Straightforward implementation. Superior damping performance. No passive component requires.	Vulnerable to f_r variations. Control bandwidth is limited by cutoff frequency. Low frequencies affect small phase margin.

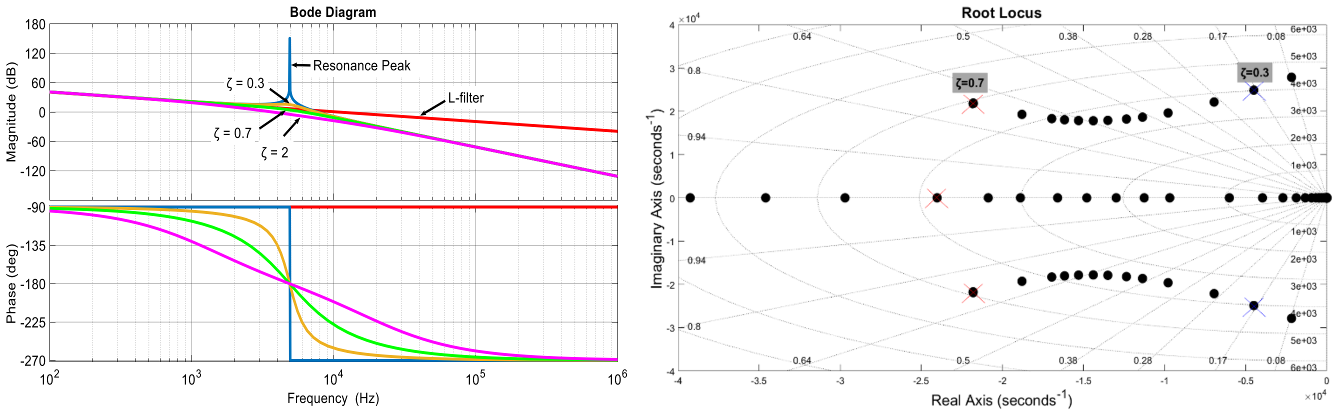

(a) (b)

Fig. 5 Diagrams of the active damping method obtained through various damping coefficients: (a) Bode plot and (b) root locus

The obtained gain margin G_m and phase margin P_m with ζ at 0.7 correspond to 5 dB/dec and 20/dec dB, respectively. With the rated power of a distributed generation of 5.5 kVA and the high switching frequency of 12 kHz, the damping coefficient of 0.7 is sufficient to handle the filter's design procedure. This means that stability is guaranteed even under significant inverter-side inductor variations. In addition, the resonance peak can be attenuated, along with the gain response, as a sizeable proportional gain would force the real closed-loop pole to move further away from the imaginary axis. The conjugate poles that move closer toward the right half-plane would make the system become gradually unstable.

4.3. The designed LCL filter's performance

The designed *LCL* filter is tested through simulation software via MATLAB/Simulink tool. The simulation results are obtained for a three-phase PWM inverter with the parameters listed in Table 2. The grid-side current with increased damping resistance R_{D3} of 1 Ω is shown in Fig. 8(b). Notice that the current magnitude is about 15 A; however, as can be seen, the distortion of the grid-side current in Fig. 8(b) is relatively more severe than that in Fig. 8(a). Therefore, even with a small value ($0 \leq R_D \leq 1$) of damping resistance, it is unable to achieve an ideal output current even in ideal conditions. In addition, it contains considerable damping losses, which are proportional to the increase in the damping resistance.

Meanwhile, Fig. 7 shows the resulting current for the active damping method with 0.7 damping coefficient. Notably, the obtained waveforms depict a pure sinusoidal waveform as in Fig. 6. For comparison, Fig. 8 displays the comparison of the yielded currents and voltages (I_{RD3} vs. I_{AD} and V_{RD3} vs. V_{AD}) for both the damping resistor and the digital filter. As can be seen, regardless of the increase in the damping factor, smoother system current flow and voltage are observed. Notably, the background distortion in I_{AD} as well as in V_{AD} can be diminished with the help of adequately designed *LCL* filter. As a result, the current harmonics component can be attenuated at the switching frequency, and pure sinusoidal waveform can be simultaneously provided. Thus, the stability margin of the overall system is guaranteed.

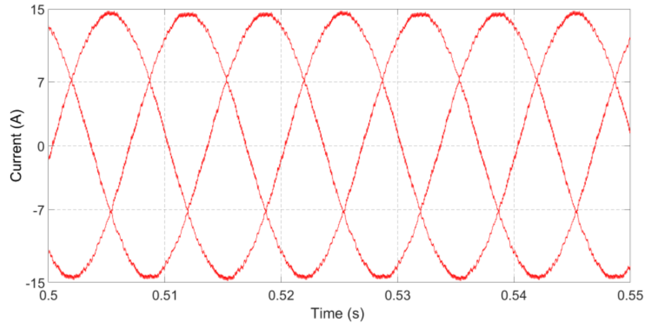

(a)

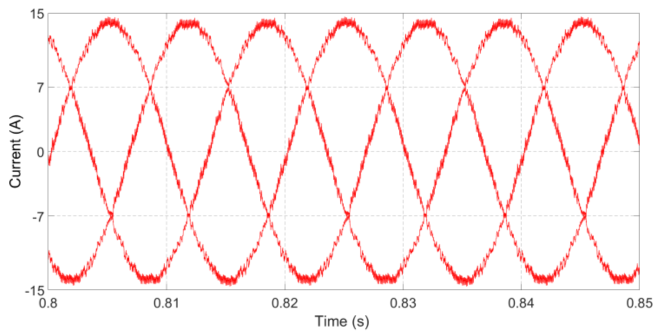

(b)

Fig. 6 Simulated current waveforms with R_D-C_f: (a) $R_D = 0.1$ Ω and (b) $R_D = 1$ Ω

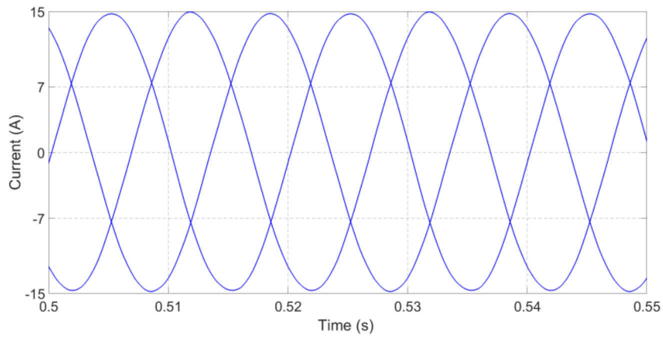

(a)

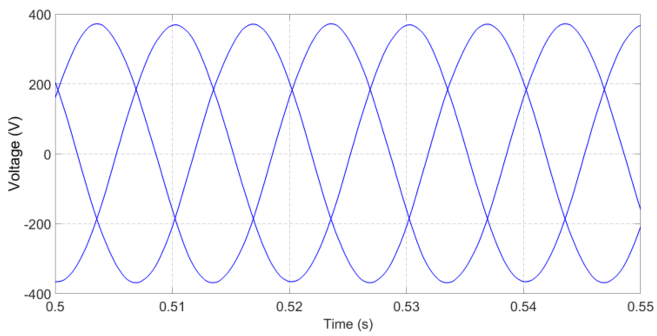

(b)

Fig. 7 Simulated current waveforms for active damping method: (a) grid-side current (I = 15A) and (b) grid-side voltage (V = 372 V)

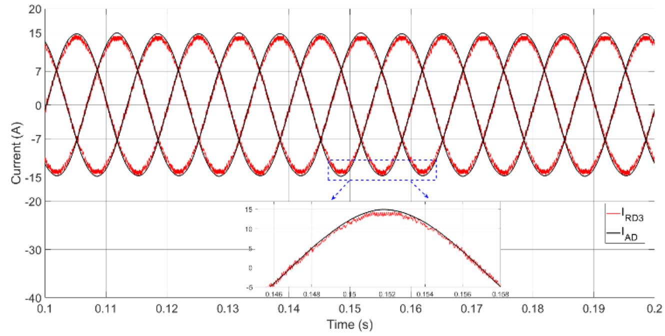

(a)

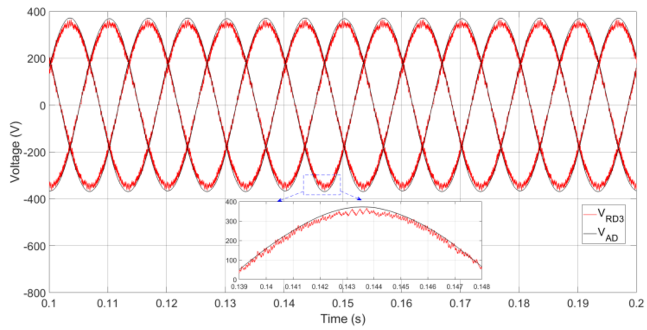

(b)

Fig. 8 Comparison of simulated waveforms with damped *LCL*: (a) grid-side current and (b) grid-side voltage

In the case of current harmonics distortion, which results in the background current at the grid side, the FFT analysis tool has been used to verify the ability to attenuate current distortion, and Fig. 9 displays the outcomes. The THD for the passive damping approach with damping resistance selected at R_D to be 1 Ω is about 3.89%. Meanwhile, the active damping method indicates 0.93% of THD_i. Notably, the largest switching frequency's current harmonic component is 70% on the converter side, whereas it is 20% on the grid side. Significantly, the grid current's THD relatively decreases and is well below 5%, which satisfies the IEEE 519-1992 Standard [28]. The performance of the designed *LCL* filter is stable with a sufficient number of inductors and capacitor. It can be seen that the grid-side current introduced by the active damping has an excellent ability to attenuate current distortion. Overall, the harmonics analysis significantly displays the effectiveness of the designed filter.

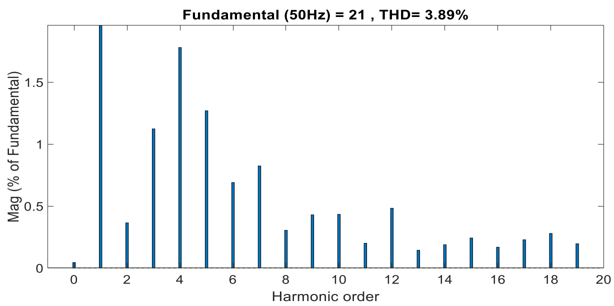

(a)

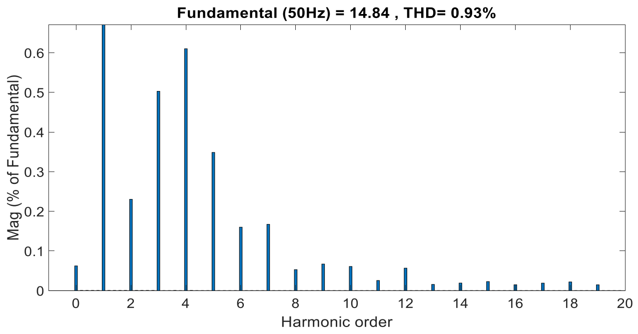

(b)

Fig. 9 THD analysis of *LCL* filter's current: (a) inverter-side and (b) grid-side

5. Conclusion

The step sequence for passive and active damping methods that comply with the systematic design methodology for the *LCL* filter in the grid-connected inverter is proposed for a better design of the *LCL* filter for the inverter-grid system. The *LCL*-type filter introduces stability; thus, passive and active internal damping stability analyses have been conducted to verify the suitable *LCL* filter's parameter values with minimum harmonics pollution. The passive damping method offers robust system stability and has a direct implementation. Even with these advantages, it still experiences high damping losses along with power losses due to the large resistance values. Therefore, active damping is proposed for high-frequency attenuation as well as for ensuring better stability of the overall system. Through simulation results, active damping is a promising approach to satisfy the *LCL* filter's design requirement with its significant feature of counteracting the high resonance peak. Adequate controller gains can be determined accordingly (when considering an incorporated controller loop). Further studies could acknowledge the exceptional performances, especially when considering the external line impedance at the grid-side power converter, and will be discussed in the next paper.

Acknowledgements

This work was supported and financed by the UTHM Research Management Centre Fund E15501, and postgraduate research grant, GPPS under VOT number H538. The authors would like to thank the Advanced Control Power Converter Team for the conducted research work.

References

[1] J. Meckling, T. Sterner, and G. Wagner, "Policy sequencing toward decarbonization," *Nature Energy*, vol. 2, no. 12, pp. 918–922, 2017.

[2] Y. W. Li and C. Kao, "An Accurate Power Control Strategy for Power-Electronics-Interfaced Distributed Generation Units Operating in a Low-Voltage Multibus Microgrid," *IEEE Transactions on Power Electronics*, vol. 24, no. 12, pp. 2977–2988, 2009.

[3] A. Ketabi, S. S. Rajamand, and M. Shahidehpour, "Power sharing in parallel inverters with different types of loads," *IET Generation, Transmission & Distribution*, vol. 11, no. 10, pp. 2438–2447, 2017.

[4] D. S. Ochs, B. Mirafzal, and P. Sotoodeh, "A method of seamless transitions between grid-tied and stand-alone modes of operation for utility-interactive three-phase inverters," *IEEE Transactions on Industry Applications*, vol. 50, no. 3, pp. 1934–1941, 2014.

[5] Y. Han *et al.*, "Modeling and Stability Analysis of LCL-Type Grid-Connected Inverters: A Comprehensive Overview," *IEEE Access*, vol. 7, pp. 114975–115001, 2019.

[6] A. Reznik, M. G. Simoes, A. Al-Durra, and S. M. Muyeen, "LCL Filter design and performance analysis for grid-interconnected systems," *IEEE Transactions on Industry Applications*, vol. 50, no. 2, pp. 1225–1232, 2014.

[7] M. Azri and N. A. Rahim, "Design analysis of low-pass passive filter in single-phase grid-connected transformerless inverter," *International Journal of Renewable Energy Research*, pp. 25–31, 2011.

[8] O. Hemakesavulu, N. Chellammal, S. S. Dash, and S. Lalitha, "A new PR-D (Proportional Resonant and Derivative) controller for resonance damping in a grid connected reverse voltage topology multi-level inverter," *2017 6th International Conference on Renewable Energy Research and Applications, ICRERA 2017*, vol. 2017-January, pp. 653–658, 2017.

[9] V. Blasko and V. Kaura, "A novel control to actively damp resonance in input LC filter of a three-phase voltage source converter," *IEEE Transactions on Industry Applications*, vol. 33, no. 2, pp. 542–550, 1997.

[10] Y. W. Li, "Control and resonance damping of voltage-source and current-source converters with LC filters," *IEEE Transactions on Industrial Electronics*, vol. 56, no. 5, pp. 1511–1521, 2009.

[11] H. Azani, A. Massoud, L. Benbrahim, B. W. Williams, and D. Holiday, "An LCL filter-based grid-interfaced three-phase voltage source inverter: Performance evaluation and stability analysis," *IET International Conference on Power Electronics, Machines and Drives*, pp. 1–6, 2014.

[12] Y. Tang, P. C. Loh, P. Wang, F. H. Choo, F. Gao, and F. Blaabjerg, "Generalized design of high performance shunt active power filter with output LCL filter," *IEEE Transactions on Industrial Electronics*, vol. 59, no. 3, pp. 1443–1452, 2012.

[13] M. H. Mahlooji, H. R. Mohammadi, and M. Rahimi, "A review on modeling and control of grid-connected photovoltaic inverters with LCL filter," *Renewable and Sustainable Energy Reviews*, vol. 81, no. August 2017, pp. 563–578, 2018.

[14] N. G. M. Thao, K. Uchida, K. Kofuji, T. Jintsugawa, and C. Nakazawa, "A comprehensive analysis study

about harmonic resonances in megawatt grid-connected wind farms," *3rd International Conference on Renewable Energy Research and Applications, ICRERA 2014*, pp. 387–394, 2014.

[15] M. . Hamad, K. . Ahmed, and A. . Madi, "Current Harmonics Mitigation using a Modular Multilevel Converter-Based Shunt Active Power Filter," *5th International Conference on Renewable Energy Research and Applications*, vol. 5, pp. 755–759, 2016.

[16] R. S. Munoz-Aguilar, J. Rocabert, I. Candela, and P. Rodriquez, "Grid resonance attenuation in ling lines by using renewable energy sources," *6th International Conference on Renewable Energy Research and Applications*, vol. 5, pp. 429–434, 2017.

[17] M. Ferrari, "GSC control strategy for harmonic voltage elimination of grid-connected DFIG wind turbine," *3rd International Conference on Renewable Energy Research and Applications, ICRERA 2014*, pp. 185–191, 2014.

[18] F. Mulolani, A. Althobaiti, and Y. Alamoudi, "Notch-Filter Active Damping of LCL Filter Resonance in a Grid-connected Inverter with Variable Grid Inductance," *2019 Advances in Science and Engineering Technology International Conferences, ASET 2019*, pp. 1–6, 2019.

[19] N. Zhang, H. Tang, and C. Yao, "A systematic method for designing a PR controller and active damping of the LCL filter for single-phase grid-connected PV inverters," *Energies*, vol. 7, no. 6, pp. 3934–3954, 2014.

[20] M. Y. Park, M. H. Chi, J. H. Park, H. G. Kim, T. W. Chun, and E. C. Nho, "LCL-filter design for grid-connected PCS using total harmonic distortion and ripple attenuation factor," *2010 International Power Electronics Conference - ECCE Asia -, IPEC 2010*, pp. 1688–1694, 2010.

[21] I. Chtouki, M. Zazi, M. Feddi, and M. Rayyam, "LCL filter with passive damping for PV system connected to the network," *Proceedings of 2016 International Renewable and Sustainable Energy Conference, IRSEC 2016*, no. September 2018, pp. 692–697, 2017.

[22] L. R. Srinivas and K. S. Rajesh, "Design & Analysis of Passive Damping LCL Filter for Power Quality Improvement Using SAPF Based on Artificial Intelligent," *International Journal of Advanced Research in Electrical, Electronics and Instrumentation Engineering*, vol. 1, pp. 5246–5260, 2016.

[23] Y. Tang, W. Yao, P. C. Loh, and F. Blaabjerg, "Design of LCL Filters with LCL Resonance Frequencies beyond the Nyquist Frequency for Grid-Connected Converters," *IEEE Journal of Emerging and Selected Topics in Power Electronics*, vol. 4, no. 1, pp. 3–14, 2016.

[24] Q. Zhao, F. Liang, and W. Li, "A new control scheme for LCL-type grid-connected inverter with a Notch filter," *Proceedings of the 2015 27th Chinese Control and Decision Conference, CCDC 2015*, pp. 4073–4077, 2015.

[25] G. Hu, C. Chen, and D. Shanxu, "New active damping strategy for LCL-filter-based grid-connected inverters with harmonics compensation," *Journal of Power Electronics*, vol. 13, no. 2, pp. 287–295, 2013.

[26] R. Peña-Alzola *et al.*, "Robust Active Damping in LCL-Filter-Based Medium-Voltage Parallel Grid Inverters for Wind Turbines," *IEEE Transactions on Power Electronics*, vol. 33, no. 12, pp. 10846–10857, 2018.

[27] M. Ben Saïd-Romdhane, M. W. Naouar, I. Slama-Belkhodja, and E. Monmasson, "Indirect sliding mode power control associated to virtual-resistor-based active Damping method for LLCL-filter-based Grid-connected converters," *International Journal of Renewable Energy Research*, vol. 7, no. 3, pp. 1155–1165, 2017.

[28] C. C. Gomes, A. F. Cupertino, and H. A. Pereira, "Damping techniques for grid-connected voltage source converters based on LCL filter: An overview," *Renewable and Sustainable Energy Reviews*, vol. 81, no. January 2017, pp. 116–135, 2018.